High-Resolution Inner-Shell Photoabsorption and Dissociation of Ozone

S. Stranges*

Dipartimento di Chimica, Universita' di Roma "La Sapienza" ed Unita' INFM, P.le A. Moro 5, I-00185 Rome, Italy

M. Alagia

TASC−INFM, Area Science Park, Basovizza I-34012, Trieste, Italy

G. Fronzoni and P. Decleva

Dipartimento di Scienze Chimiche, Universita' degli Studi di Trieste, Via L. Giorgieri 1, I-34127, Trieste, Italy

Received: October 23, 2000; In Final Form: January 4, 2001

The total-ion-yield (TIY) spectrum of ozone has been recorded in the K-edge region for the first time with high photon energy resolution and without significant O_2 contamination. Spectral features have been clearly observed in the high energy region below the two ionization thresholds. The assignment for the core excitation processes from the "terminal" and "central" oxygen atoms, given for the first time in the whole spectral range, is based on high level ab initio calculations. The QDPTCI (quasidegenerate perturbation theory configuration interaction) theoretical approach provided an excitation energy pattern and photoabsorption oscillator strengths that were found in good agreement with the experimental TIY spectrum. The decay dynamics of the core excited resonant states is shown to be strongly dependent on the σ/π antibonding character of the virtual MO involved in the excitation process.

Introduction

The ozone molecule has been the subject of a high number of investigations because of its importance in human life as a solar radiation filter in the Earth's upper atmosphere. Although considerable attention has been paid to the reactivity and spectroscopy of this molecule, relatively little is known about core photoexcitation and photoionization processes. To our knowledge, only a few experimental and theoretical studies on the photoabsorption, photodissociation, and resonant Auger spectroscopy of O_3 in the K-edge region have been carried out, namely by Gejo et al.,[1,2] Naves de Brito et al.,[3] and by Wiesner et al.[4] These recent works follow the previous X-ray photoelectron spectroscopy (XPS) study by Banna et al.[5] Ozone is a C_{2v} symmetry molecule in the ground state with two chemically different oxygen atoms, the "central" and the two "terminal" ones. The large difference in the chemical shift of the two kinds of atoms, 4.7 eV as measured by XPS,[5] suggests that site-specific core excitation processes and decay dynamics of inner-shell resonant states could be selectively studied using high-resolution photon sources.

High resolution, intense, and linearly polarized light, currently provided by third generation synchrotron radiation (SR) undulator beamlines,[6] has been used in this work to study inner-shell excitation and dissociation processes in the ozone molecule using time-of-flight (TOF) mass spectrometry (PEPICO) and angle-resolved photofragment ion yield spectroscopy. The latter technique has been proved to be an effective method to characterize core excited states formed by photoabsorption in small molecules.[7−10] In the present work the very low O_2 contamination of the ozone sample allowed new features to be clearly observed in the high energy spectral region. If oxygen is present,[1,2] this region contains highly structured and intense Rydberg features of O_2 that overlap bands of O_3 making their observation and assignment difficult.

The excitation energies and photoabsorption oscillator strengths have been calculated by high level ab initio methods. It has long been known that the theoretical description of the electronic structure of O_3 requires an explicit account of the correlation effects; in fact already the ground state has significant multi-reference character due to the strong mixing of the HOMO−LUMO excitation and also several low-lying transitions have significant double excitation character. Besides the electronic correlation, the description of core excited electronic states also requires the inclusion of the strong relaxation effects on the valence orbitals following core hole formation. The ab initio configuration interaction (CI) approach is able to account for both these effects in a very effective way. The relaxation can be explicitly included by employing different orbital sets optimized for the ground and the core ionized states while the correlation effects can be described at various levels of approximation. The simplest model for the description of core excitations is the relaxed 1h−1p CI which includes the single excitations from the specific core level of the probed atom and the important coupling between different channels in the case of degenerate core holes (2p for example). This scheme has proved to be adequate to describe the main structures of the XAS spectra both of simple and rather complex molecules.[11,12] A more accurate description of the oscillator strength distribution among the discrete valence and Rydberg transitions can be achieved by including higher order correlation effects making use of perturbative schemes at the CI level. In this work we

* Corresponding author. E-mail: stranges@axcasp.caspur.it. Tel. +39−06−49913362. Fax. +39−06−490324.

10.1021/jp003902v CCC: $20.00
Published on Web 03/06/2001

employed the second-order quasi degenerate perturbation theory approach (QDPT-CI)[13] which has been shown to be very effective if a detailed analysis of the individual levels is required, in particular in the Rydberg region, as reported in previous theoretical investigations.[14]

Since core-hole localization and relaxation effects, and electron correlation have been included in the theoretical method, more accurate excitation energies and, for the first time, transition probabilities have been calculated for inner-shell absorption processes in the ozone molecule. Therefore, a reliable and more detailed assignment of the experimental resonant features observed in the TIY spectrum in the K-edge spectral region is here proposed.

Experimental Section

Experimental Spectra. The experiment was carried out at the ARPES end station of the Gas-Phase undulator beam line at ELETTRA.[6] The photon resolution used in the oxygen K-edge region was about 50 meV, and the beam spot size in the ionization region was about 0.3 × 0.3 mm. All spectra were recorded using a PEPICO (photoelectron-photoion-coincidence) time-of-flight spectrometer mounted on a rotating support to vary the angle of detection with respect to the polarization plane of the linearly polarized synchrotron light. The ozone effusive inlet system consisted of a small Teflon pipe with its end lined externally with a grounded copper shield close to the ionization region. The gas inlet system was mounted on the rotating support with its axis perpendicular to the direction of the photon beam. The spectrometer consists of the extraction region, defined by two gold meshes (90% transmission), the ion acceleration section, the ion drift tube, the ion detector (a MCP "Z" three-element assembly), and a large input cone channeltron multiplier, mounted close to the extraction region, as the electron detector. Extraction and acceleration electric fields were chosen to minimize fast electron and fragment-ion detection losses. The constancy of total electron and ion yield spectra were checked by recording spectra at different detection angles (0°, 54.7°, and 90°). The spectrometer was operated in two different modes: (a) the electric field free mode, to record the fragment-ion yield (FIY) as a function of the angle of detection, and therefore to study the anisotropy of the fragment-ion emission from the core-excited resonant states, and (b) the PEPICO mode, recording mass resolved TOF spectra. In this latter mode the photoelectron start and ion stop signals were sent to a time-to-pulse-height converter (ORTEC, model 467). The start/stop time interval was converted into a voltage analogic signal that was stored in the memory of a qVt multichannel analyzer (LeCroy model 3001). The ion peak areas, namely, the sum of the channel contents contributing to each of the TOF ion peaks, were stored separately into scaler channels (LeCroy, model 2551) as a function of the photon energy, thus allowing the ion-yield (IY) spectra to be recorded. The total number of detected ions was stored in a different channel enabling the total ion-yield (TIY) to be registered. Also, ion−ion coincidence events, due to double- and multiphotoionization processes, were recorded as a function of the photon energy by selecting ion signals from different parts of the TOF mass spectrum and processing them using AND logic units.

The photon energy calibration was based on the intense and sharp bands obtained in high-resolution O_2 ion yield spectra recorded, *simultaneously* with the ozone spectra, in an absorption cell located behind the experimental chamber and differentially pumped. The energy values used for the calibration were those reported in high-resolution absorption and EELS works.[15,16] All spectra were normalized with respect to the incident photon flux, measured by a silicon photodiode (IRD AXUV-100) mounted at the end of the experimental apparatus, and to small and slow changes in the ozone pressure that was monitored continuously and stored during the photon energy scans.

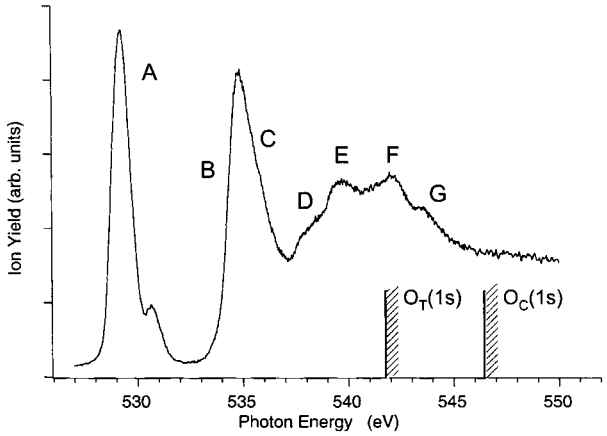

Figure 1. Oxygen K-edge total ion yield (TIY) spectrum of ozone. The measured O 1s photoionization thresholds, 541.75 and 546.44 eV, are also reported. The weak feature at 530.7 eV is due to the O 1s → π^* transition of a small amount of O_2 present in the sample.

The sample was produced according to an established method[17] by discharging pure O_2 in a commercial ozone generator and trapped on silica gel at low temperature in an acetone-dry ice slush bath. The residual O_2 was removed by long pumping just before the experiment and the effusive gas inlet system was designed to avoid contact between metal surfaces and the ozone gas. The O_2 contamination in the first measurements (spectrum in Figure 1) was estimated to be about 8%, as measured by the $\pi^*(O_2)/\pi^*(O_3)$ peak area ratio. The O_2 relative concentration decreased slightly during the experiment. The O_2 contribution to the ozone spectra was estimated by recording pure O_2 spectra at different detection angles in the same experimental conditions used for the ozone. The tests showed that this contribution was less than 3% of the total signal in the 533−547 eV spectral region and therefore negligible in this energy range.

Ab Initio Calculations. The CI calculations of the discrete excited states have been performed employing the correlated basis set cc-pVTZ (correlation consistent polarized valence triple zeta) proposed by Dunning,[18] i.e., the (10s,5p,2d)/(5s,3p,2d) set. The set has been enlarged by adding some diffuse functions needed to describe the transitions toward Rydberg orbitals. In particular we have added four diffuse s,p functions with exponents obtained with the even tempered criterion ($\beta = 3$) and five d functions, the first with exponent $\alpha_d = 0.2144$ and the last four with the same exponents as the last four p functions. The final basis for the oxygen is the (9s,7p,7d) set, which is employed for describing the O atom on which the core hole is localized; for the other two oxygen atoms the original (5s,3p,2d) set is employed. Calculations have been performed employing a fully orthogonal basis obtained by preliminary atomic calculations with the GTO basis employed. This eliminates interatomic nonorthonormality rendering the AO composition of the MOs more transparent.

Separate calculations have been performed for excitations from the O 1s orbital of the central oxygen atom (O_C) and the terminal one (O_T). In each case SCF orbitals for the corresponding O 1s core hole state have been employed. This treatment, in the case of core excitations, is a standard approach for taking into account the strong relaxation associated with

the core hole formation at the zero order, and giving a substantially improved description of the spectra calculated at the 1h−1p CI level. In the case of the two equivalent terminal oxygen atoms (O_T), the core hole has been localized on a single center and the molecular symmetry reduced accordingly. Coupling between excitations from different holes has been neglected, as it is usually assumed negligible because of the small value of the matrix elements involving the strongly localized holes that are spatially well separated.

The core excited spectra are first calculated in the 1h−1p CI scheme allowing all the single excitations from the fixed 1s core hole localized separately on the central and on the terminal nonequivalent oxygen atoms.

The highly correlated computational scheme used for the QDPTCI calculations has been described in detail in previous papers.[19,20] Here we report only the computational strategy adopted. The main point is the choice of the zero order reference space, R, which is generated by the most interacting configurations plus all other strongly interacting or lower lying configurations. A good starting point is the relaxed 1h−1p CI scheme, which comprises all the singly excited configurations from the fixed core hole and has relatively modest dimensions. The reference space is completely diagonalized and the lowest physically important eigenvectors of R define the zero order Hamiltonian and a corresponding smaller zero order P space. The R space can be enlarged by inclusion from the Q perturbing space of the possible intrusive configurations (which are not uncommon in core excited spectra) and further perturbative selection with a threshold coefficient *c*, previously fixed. In the present case the full 3h−3p space is employed as perturbing Q space while the threshold coefficient used is $c = 0.010$. This value has proven to be accurate in previous studies. With this *c* value iterative selection on the perturbing Q space for the generation of the final reference space has been performed before applying the QDPT. The same scheme has been also applied to the ground state. Note that for the description of the core excited states we enforce a single hole in the relevant core orbital (1s) while such a restriction does not apply to the GS. This difference in configuration spaces may cause a slight nonorthogonality between the ground and the excited state wave functions of the same symmetry, despite employing the same orbital set. For this reason the transition moments are reported only in the dipole velocity form

$$f = \frac{2}{3}\omega^{-1}\mathrm{M}^2, \quad \bar{\mathrm{M}} = \langle \psi_\mathrm{f}, \bar{\nabla}\psi_\mathrm{i} \rangle$$

which is less affected by the nonorthogonality problem. SCF, CI, and transition moments calculations are performed with the MELDF set of programs.[21] The ground-state experimental equilibrium geometry of O_3 has been employed in all calculations.

Results and Discussion

Experimental Spectra. We would like to remind first the electronic structure of the ozone molecule and some symmetry considerations that are useful for describing the results obtained in this work and their discussion. The ground-state electronic structure of O_3 (C_{2v} symmetry) in the molecular orbital picture can be described as follows:

$1a_1^2\, 2a_1^2\, 1b_2^2$ core MOs (O 1s AOs)

$3a_1^2\, 2b_2^2\, 4a_1^2$ inner valence MOs (O2s AOs)

$5a_1^2\, 1b_1^2\, 3b_2^2\, 4b_2^2\, 6a_1^2\, 1a_2^2\, 2b_1^0\, 7a_1^0\, 5b_2^0$ valence MOs (O2p AOs)

The innermost $1a_1$ core orbital is the 1s central oxygen AO (O_C 1s) while the $2a_1$ and $1b_2$ are almost purely even and odd combinations of the 1s terminal oxygen AOs (O_T 1s). The inner valence part comprises the $3a_1$, $2b_2$ and $4a_1$ MOs derived from the 2s AOs of the oxygen atoms, while the 2p AOs give rise to the two $5a_1$ and $3b_2$ MOs with σ bonding character, the two nonbonding $6a_1$ and $4b_2$ MOs which represent the terminal O_T lone pairs, and the two $7a_1$ and $5b_2$ unoccupied MOs with σ^* antibonding character. The lowest unoccupied σ^* MO is the $7a_1$. The $1b_1$ occupied MO is the O_C $2p(\pi)$ orbital while $1a_2$ and $2b_1$ are combinations of the O_T out-of-plane 2p AOs. The $1a_2$ MO is occupied in the HF description of the ground state, while $2b_1$ is the lowest unoccupied MO (π^*), the LUMO, and represents the complement of the $1b_1$ π bonding orbital.

The most intense transitions expected in the K-edge photoabsorption and the TIY spectrum of O_3 are electron excitations from the core MOs into the three relatively compact unoccupied valence MOs. Weaker transitions into the more diffuse Rydberg orbitals are expected at higher photon energies below the two O 1s ionization thresholds. Within the minimal basis set scheme given above only the stronger valence excitations can be described. A more refined theoretical picture is needed to include Rydberg transitions and the possible valence/Rydberg character mixing for high energy excitation processes. Also, when we consider excitations where the 1s core hole is localized on the terminal oxygen atom (O_T), the C_{2V} symmetry is broken and the C_s symmetry has to be used in considering the O_T MOs; in particular the three unoccupied valence orbitals become 3a″ (π^*), 11a′ (σ^*), and 12a′ (σ^*).

The experimental high-resolution TIY spectrum of ozone in the K-edge region is reported in Figure 1. Two intense bands at low energies dominate the whole spectrum. The former at 529.25 eV is due to the O_T (1s) → 3a″ (π^*) excitation while the latter, centered at 534.9 eV with intensity approximately double that of the first band, is ascribed to the two valence transitions O_C (1s) →$2b_1$ (π^*) and O_T (1s)→11a′ (σ^*). This assignment is in accord with a recent report [1]. The fwhm observed for the first peak, 1.09 eV, is larger than the one observed in the corresponding π^* resonance peak of O_2 (0.75 eV) that was recorded simultaneously in the absorption cell. This finding can be explained in terms of a more extended unresolved vibrational envelope in the larger O_3 molecule. In contrast with O_2, no vibrational structure was observed in the O_3 spectrum even using photon energy resolution better than 50 meV. As for the second band, the composite nature of the peak has been investigated experimentally by us in some detail. The fragment ion yield (FIY) spectrum recorded at different detection angles with respect to the polarization plane of the light, namely at 0°, 54.7°, and 90°, and using a narrow photon band-pass is reported in Figure 2. The detection acceptance angle was about 4°. The spectrum at 54.7° (the magic angle) is not shown in the figure since it was very similar to the TIY spectrum of Figure 1. The angular distribution of the fragment ion emission from the two different valence resonances, with π^* and σ^* characters, is remarkably different. It is clear from the strong change in the peak shape of the second band on going from 90° to 0° that the O_T (1s)→11a′ (σ^*) resonance decays emitting fragment ions preferentially in the polarization plane of the light (0°). This does not seem to be the case for the O_C (1s)→$2b_1$(π^*) resonance. Furthermore, TOF mass spectra have been recorded with different angles of detection and at different

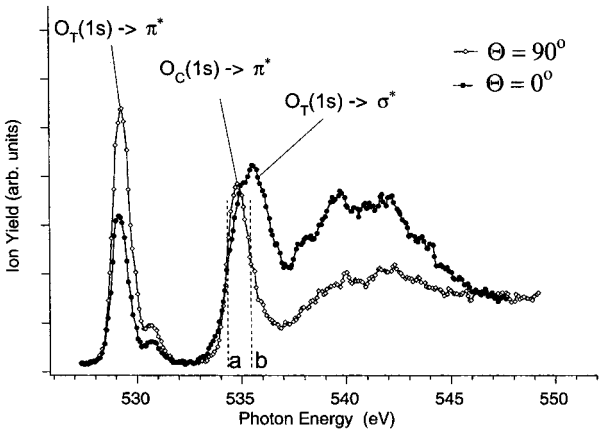

Figure 2. Oxygen K-edge fragment ion yield (FIY) spectrum of ozone recorded at 0° and 90° with respect to the polarization plane of the light. The spectrum at the magic angle (54.7°), not shown, is very similar to the TIY spectrum (Figure 1).

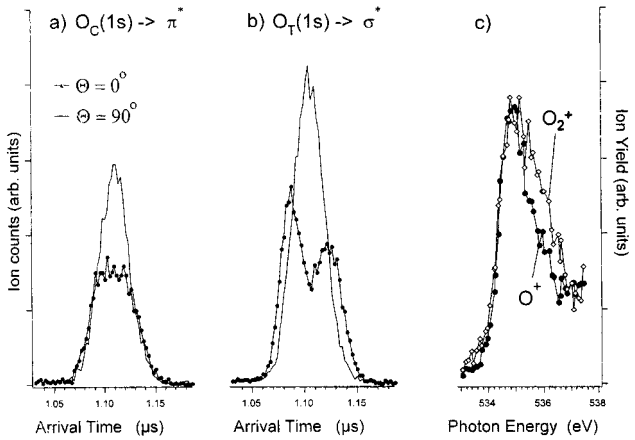

Figure 3. (a), (b) O_2^+ fragment ion time-of-flight spectrum recorded parallel (0°) and perpendicular (90°) to the polarization plane of the light at photon energies labeled (a) and (b) in Figure 1. (c) O_2^+ and O^+ PIY spectra recorded for the second experimental band. The O^+ yield is due to both O^+ and O_2^{2+} ions.

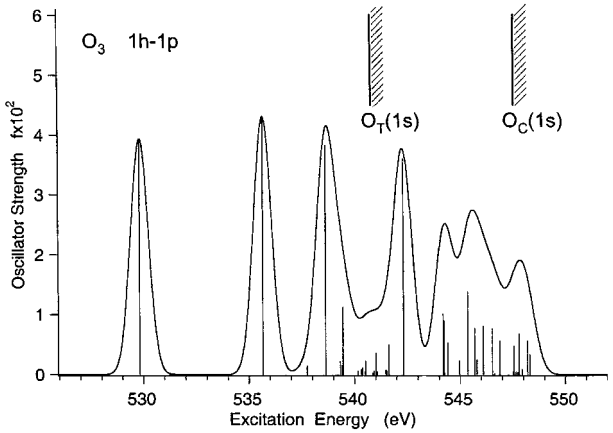

Figure 4. QDPTCI calculated O 1s core excitation spectrum of O_3. Lines are convoluted with Gaussians of 1.0 eV fwhm. The experimental O 1s photoionization thresholds are shown.

photon energies, from the low to the high energy side of the band, as well as at the energy corresponding to the top of the band observed in the TIY spectrum. The arrival time distribution of the O_2^+ fragment ion, namely the O_2^+ peak shape in the TOF spectra, obtained at the energies labeled (a) and (b) in Figure 2 are reported in Figures 3a and 3b. The photon energies were chosen to probe *selectively* the two different resonances. In the case b) the arrival time distribution is described by a single symmetric peak when the detection axes is perpendicular to the polarization plane (90° curve) while it displays a double-peak shape with forward and backward parts when the detection axis is in the polarization plane (0° curve). This finding is typical of an angular distribution with a maximum at 0° and characterized by a high β (asymmetry parameter) value. In the case (a) the difference in peak shape is much less pronounced suggesting a more isotropic angular distribution. From the analysis of the O_2^+ TOF peak profiles using methods published recently,[22,23] asymmetry parameters of 0.55 ± 0.2 and 1.15 ± 0.2 have been derived for the two photon energies labeled (a) and (b) in Figure 2. These two positive values do not agree with the $\beta = 0$ value reported in a previous study[2] obtained at the energy corresponding to the peak center. While the discrepancy at the higher photon energy (mainly σ^* character) can be due to the higher energy resolution, thus higher state selectivity, of the present experiment, the reason for the difference observed at 534.35 eV is unclear. In contrast the time-of-flight spectrum recorded on the lowest energy resonance (O_T 1s$\rightarrow\pi^*$, not shown) yields a β value of -0.4 ± 0.2. The latter value is in good agreement with the result reported previously by Gejo et al.[2] We plan to examine the angular distribution of the fragments and its photon energy dependence in more detail in a future experiment using a three-dimensional time-of-flight technique.

Partial ion yield spectra have been recorded in the K-edge region. All ion channels have been stored simultaneously as a function of the photon energy. The O_2^+ and O^+ PIY spectra in the region of the second band are reported in Figure 3c. The O_2^+/O^+ ratio increases significantly on going from the π^* to the σ^* resonance thus providing a further experimental evidence of the existence of more then one state contributing to the second experimental band. The photodissociation decay channels yielding two ions have been investigated by detecting ion−ion coincidence events as a function of the photon energy. The O_2^+/O^+ decay channel has been found to be by far the most important one. These coincidence data, however, in the context of this work, do not add new information concerning the photoabsorption energetics and therefore are not reported here.

At energies higher than 537 eV the TIY spectrum (Figure 1) displays a broad feature that extends over about 8 eV. Four bands, labeled D−G in the figure, are observed in this spectral region at 537.9, 539.7, 542.0, and 543.8 eV, respectively. Bands D and E are located below the first ionization threshold (O_T 1s), while F and G are between the two thresholds. In this region transitions into σ^* valence and Rydberg unoccupied orbitals are expected. The assignment of this part of the spectrum will be guided by the results of the ab initio calculations.

Ab Initio Calculations. The calculated O 1s excitation spectrum using the QDPTCI and 1h-1p CI methods is reported in Figures 4 and 5. The QDPTCI oscillator strengths and the excitation energies relative to the first calculated excitation energy (O_T 1s$\rightarrow\pi^*$ transition) are collected in Table 1 together with the experimental data. The experimental excitation energies converge to the O_T 1s and O_C 1s ionization thresholds located at 541.75 and 546.44 eV respectively, as measured in this work at 565.0 eV photon energy by XPS using O_2 as a calibration gas.[24]

The spectral region at energies higher than the second band has not yet been interpreted systematically, and to our knowledge no accurate theoretical calculations with an extended basis set are present in the literature. Therefore, the present theoretical study improves the understanding of the high energy excitation

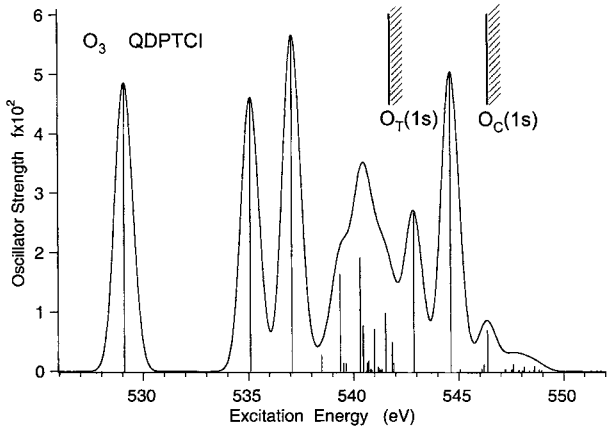

Figure 5. 1h-1p CI calculated O 1s core excitation spectrum of O_3. Lines are convoluted with Gaussians of 1.0 eV fwhm. The calculated DSCF O 1s photoionization thresholds, 547.65 and 540.84 eV, are shown.

processes which characterize the threshold regions. It is well-known that even in relatively small molecules a detailed analysis of the individual excited levels can prove difficult, as well as the distinction between valence and Rydberg structures, because of possible mixing of orbitals of the same symmetry to form excited states of composite valence-Rydberg character. In this respect, the theoretical calculations represent an essential support to determine the nature of the electronic transitions and to assign the related spectral features.

Let us consider in detail the more accurate QDPTCI results (Table 1 and Figure 4). The calculated spectrum (Figure 4) compares well with the experimental one and clearly shows the complexity of the higher energy part which has contributions from a large number of lines of considerable intensity, although well defined features are clearly apparent which correspond closely to those experimentally detected. As seen in Table 1 the excitation energies of the first two lines (529.09 and 535.1 eV) compare very well with the experimental values (529.25 and 534.8 eV). Also, the intensities are well described, with the second line (O_C 1s$\rightarrow\pi^*$) only slightly less intense than the first one (O_T 1s$\rightarrow\pi^*$), as seen in Figure 1. The next line, the single intense O_T 1s$\rightarrow\sigma^*$ transition, is instead calculated to be too high by more than one eV. This discrepancy is attributed to incomplete treatment of correlation at the present QDPTCI level, which is most important for the position of the next σ^* states, as will be apparent from the comparison with the single particle 1h-1p CI results (see below). This overestimate is responsible for the large separation between the second and third calculated lines and the consequent appearance of two distinct peaks in the theoretical spectrum in place of the second wide experimental peak.

The experimental energies measured in this work for the two transitions contributing to the second band do not agree quantitatively with the values published recently.[1] The photon energy calibration method used in ref 1 was suggested to be affected by nonlinear effect.[3] Good agreement is found instead for the energy separation between the two states. In this work an energy separation of 0.95 ± 0.05 eV was obtained by fitting simultaneously the FIY spectra obtained at the three different angles 0°, 54.7°, and 90° (Figure 2). The calculated intensity of the third O_T 1s$\rightarrow\sigma^*$ transition is larger than the oscillator strength of the O_C 1s$\rightarrow\pi^*$ excitation. This is in accord with the experimental relative intensities estimated in this work for the two components contributing to the band in the TIY spectrum. The experimental relative intensities for the first three states, labeled A, B, and C in Table 1, are 1, 4.61, and 5.66, respectively. These values were obtained using a Voigt function fit where the Gaussian and Lorentzian components were used as free parameters. The fwhm (full width at half-maximum) values for the three Voigt peaks were 1.06, 1.05, and 1.48 eV for the states A, B, and C, respectively. The experimental relative intensity and the fwhm found for the B and C components of the second spectral band are close to the ones shown in Figure 1b of ref 2. The calculated oscillator strength of the O_C (π^*) and O_T (σ^*) transitions appears over-estimated with respect to the first calculated transition and also to the intensity ratio observable for the two valence experimental peaks. The discrepancies between the present theoretical and experimental data in the valence energy region indicate that possible inadequacies in the computational scheme employed can probably be due to an incomplete description of the stronger correlation effects associated with the quasi-degenerate set of the π orbitals $1b_1$, $1a_2$, and $2b_1$. The inclusion of higher excitations in the π space could be required already at the zero order level; this hypothesis is corroborated by the analysis of the results obtained at the 1h-1p CI level, which represents the starting zero order reference space in our computational scheme. As seen in Figure 5 the deficiencies affecting the 1h−1p CI description of the first three valence transitions are only partially improved at the QDPTCI level, at variance with the higher energy part of the spectrum which is completely modified in passing from the 1h−1p CI to the high correlated results.

Turning now to the high energy region of the O_3 spectrum, the experimental structures observed in this region (Figure 1, labels D−G) appear less resolved than the valence peaks; however it is possible to distinguish clearly four bands, whose relative energies are reported in Table 1 (8.65, 10.45, 12.75, and 14.55 eV). The QDPTCI results describe correctly the experimental pattern (see Figure 4) and display clearly that the calculated features derive from a large number of possible final states over which the oscillator strength is distributed. In particular, we can observe several lines of decreasing intensity converging to the O_T 1s ionization threshold followed by two more intense lines above the first threshold and a final weak structure close to the higher O_C 1s threshold. From the results reported in Table 1 it is apparent that, apart from the first three valence excitations, all the lines calculated below the first ionization threshold are due to transitions from the terminal oxygen atoms and are well separated from the transitions involving the O_C 1s orbital. This energy region is characterized by the presence of the remaining O_T σ^* valence transition as well as of transitions to Rydberg states. It has been often observed in the core excitations of several molecules[12] that a mixing between Rydberg and valence components in the final state can redistribute the oscillator strength over several transitions to mixed valence-Rydberg final states, reducing the intensity of the valence transitions. This mixing characterizes also the excited states associated with the O_T transitions, which involve final states with different contributions from valence σ^* and s, p and d Rydberg components, as we can infer from the orbital composition of the O_T 1s core hole MOs. In particular, in the case of the two final states labeled 12a′ and 13a′ (at 9.39 and 10.27 eV) the mixed valence-Rydberg character is responsible for the drop in their intensity with respect to the pure-valence transition at lower energies. Furthermore, we observe that the calculated oscillator strength of these two lines is very different: this reflects the quite different distribution of the σ^* valence contribution between the 12a′ and 13a′ MOs revealed by the orbital composition. The 12a′ virtual MO has a

TABLE 1: Experimental and Calculated O 1s Core Excitation Energies (eV) and Oscillator Strengths $fX10^2$ for O_3[a]

experimental		QDPTCI		final state		
E/label		*E*	$f \times 10^2$	symmetry	assignment	dominant character
(529.25)	A	(529.09)	4.862	A″	3a″	1s → π^* (O_T)
5.55	B	6.01	4.614	B_1	$2b_1$	1s → π^* (O_C)
6.50	C	7.99	5.661	A′	11a′	1s → σ^* (O_T)
		9.39	0.278	A′	12a′	1s → σ^* + ns (O_T)
8.65	D	10.27	1.637	A′	13a′	1s → σ^* + np (O_T)
		10.43	0.146	A”	4a″	1s → np + π^* (O_T)
		10.55	0.143	A′	14a′	1s → np + nd (O_T)
10.45	E	11.23	1.919	A′	15a′ + 19a′	1s → ns,nd + σ^*, nd (O_T)
		11.37	0.783	A′	15a′+ 19a′	1s → ns,nd + σ^*, nd (O_T)
		11.57	0.154	A′	17a′ + 19a′	1s → nd + σ^*,nd (O_T)
		11.59	0.056	A″	6a″	1s → nd (O_T)
		11.63	0.176	A′	18a′	1s → nd,ns (O_T)
		11.72	0.037	A”	7a″	1s → np (O_T)
		11.77	0.025	A′	20a′	1s → np,nd (O_T)
		11.90	0.720	A′	19a′ + 24a′	1s → σ^* + np,nd (O_T)
		12.08	0.077	A′	21a′ + 25a′	1s → nd,np (O_T)
		12.11	0.059	A′	22a′ + 23a′	1s → nd,np,ns (O_T)
		12.18	0.028	A″	9a″	1s → nd,np (O_T)
		12.25	0.038	A″	10a″	1s → np (O_T)
		12.27	0.026	A′	26a′	1s → nd,np (O_T)
		12.43	0.990	A′	30a′ + 28a′	1s → σ^*,np + nd,σ^* (O_T)
		12.74	0.500	A′	30a′ + 28a′	1s → nd,σ^* + σ^*,np (O_T)
		12.82	0.139	A′	29a′ + 30a′	1s → nd + σ^*,np (O_T)
12.75	F	13.78	2.659	A_1	$7a_1$	1s → σ^* (O_C)
14.55	G	15.53	5.022	B_2	$5b_2 + 6b_2$	1s → σ^* + σ^*,np (O_C)
		15.97	0.028	A_1	$8a_1$	1s → ns (O_C)
		17.01	0.036	B_1	$3b_1$	1s → np (O_C)
		17.11	0.117	A_1	$9a_1$	1s → ns + σ^* (O_C)
		17.29	0.698	B_2	$6b_2 + 5b_2$	1s → σ^*,np + σ^* (O_C)
		17.98	0.030	A_1	$10a_1$	1s → ns (O_C)

[a] Absolute excitation energy is given for the first line ($1s(O_T) \rightarrow \pi^*$). Excitation energies relative to first line are reported for the following transitions. The experimental O 1s (O_T) and O 1s (O_C) ionization energies measured in this work are 541.75 and 546.44 eV, respectively.

smaller contribution from the O2p atomic component with respect to the 13a′ MO and a quite important O2s component. This renders the transition from the O_T 1s orbital to the 12a′ MO unfavorable reducing drastically the oscillator strength. The calculated oscillator strength is in fact able to map the contribution to the final state of the atomic orbital carrying most of the transition moment, namely in this case the O2p atomic component. A high oscillator strength is calculated for the two transitions at 11.23 and 11.37 eV, whose final states have contributions from two strongly mixed 1h-1p configurations, the $(1s)^{-1}15a'$ and $(1s)^{-1}19a'$. While the 15a′ virtual orbital has essentially Rydberg character, the 19a′ virtual orbital is characterized by a large σ^* valence contribution responsible for the quite high oscillator strength calculated for these two excited states. In this case their different calculated intensity is associated with the different extent of the configuration mixing in the resulting final states. The remaining calculated transitions converging to the O_T 1s ionization threshold are assigned to excited states of Rydberg nature and appear very weak.

In summary, the present results indicate that the second σ^* valence orbital of the terminal oxygen atoms has an energy high enough to mix with the Rydberg orbitals giving rise to several excited states of mixed valence-Rydberg character over which the oscillator strength tends to redistribute. Finally, we can note that the O_T 1s transitions calculated in the energy range from about 9.5 eV to 13 eV reflect the first two high energy bands observed in the experimental spectrum (Figure 1, labels D and E). The main deficiency of the theoretical results derives from the over-estimate of the O_T excitation energies, as already underlined for the lowest O_T σ^* transition, which shifts the relative calculated structure toward high energy.

Let us consider now the last features falling between the two O 1s ionization thresholds. The lines calculated in this energy range are due to transitions from the O_C 1s orbital. The two strong lines at 13.78 and 15.53 eV are assigned to transitions to the $7a_1$ and $5b_2$ σ^* virtual valence MOs. The excited state at 15.53 eV is dominated by the $(1s)^{-1}$ $5b_2$ configuration with a partial contribution also from the $(1s)^{-1}6b_2$ configuration. The oscillator strengths calculated for these two lines are quite different, as it is well apparent in Figure 4, and reflect the different content of the O2p atomic component present in the $7a_1$ and $5b_2$ virtual MOs, this being much stronger in $5b_2$ than in $7a_1$. Also the $6b_2$ virtual MO has a notable O2p atomic contribution. The $7a_1$ MO is instead characterized by the presence of an important O2s component which renders the transitions from the O_C 1s orbital less favorable. It should be noted that the intensity distribution over the σ^* valence transitions from the O_C 1s orbitals is different from the one observed for the σ^* O_T ones; the higher σ^* O_C valence transition (at 15.53 eV) appears in fact much more intense than the lowest one (at 13.78) reversing the trend observed for the valence σ^* O_T transitions. Furthermore, the concentration of the calculated oscillator strength essentially on the two σ^* O_C valence transitions is related to the lack of mixing between the valence and Rydberg components, as it is apparent also from the composition of the final states (Table 1). This different behavior could be partly ascribed to the different symmetry around the core-hole at the O_T and O_C atoms.

Moreover, it is important to underline that a possible overestimate of the calculated intensities for the σ^* O_C valence transitions can be an artificial effect of using a finite basis set

in a spectral region where the "discrete" transitions from the O_C atom are embedded in the O_T 1s ionization continuum.

The small calculated structure around the O_C 1s threshold derives its intensity essentially from the transition at 17.29 eV toward a final state partly contributed from the 1h-1p $(1s)^{-1}5b_2$ configuration, which gives a partial σ^* valence character to the excited state and it is responsible for the intensity gain with respect to the other states calculated in this energy region. The tail at higher energy extends over a few eV above the O_C 1s experimental ionization threshold and is contributed from transitions toward final states with predominant Rydberg character, which show a negligible intensity. The calculated O_C transitions pattern matches well the experimental bands falling between the two ionization thresholds, apart from the overestimated intensity of the higher σ^* $(5b_2)$ transition, already commented.

As for the comparison between the QDPTCI and 1h−1p CI results (Figures 4 and 5) we observe a qualitative accord for the relative energies and intensities of the first three valence transitions; only a small improvement of the energy separation between the second and third lines is apparent on going from the 1h−1p CI to the QDPTCI spectrum. The deficiency of the simpler 1h−1p CI scheme is instead apparent in the high energy part of the spectrum where a different pattern from the QDPTCI spectrum and the experimental features is observed. In particular, the transitions near the O_T 1s ionization threshold are strongly underestimated producing a structure too close in energy to the third valence transition while most of the intensity appears above the O_T threshold; a very intense line is calculated around 542 eV and several other quite intense transitions fall at higher energy and overlap with the 1h−1p O_C 1s excitations. These give rise to the higher energy part of the last calculated structure around the O_C threshold. Generally, the 1h−1p CI scheme underestimates the oscillator strengths and redistributes the intensities over the higher excited states in a very different way. It is important to emphasize that the 1h−1p CI scheme is generally adequate to describe with a reasonably good accuracy the discrete excitation structures of several systems,[11,12] as already stressed, and therefore the low performance in describing the high energy part of the ozone spectrum is a further confirmation of the need to correctly include the strong correlation effects present in this molecule.

In light of the assignment given for all the resonant states below the two ionization thresholds, it is interesting to note in Figure 2 that resonances with σ^* character preferentially decay emitting fragment ions parallel to the polarization plane of the light (curve $\Theta = 0°$). A different behavior is observed for the two π^* resonances, as is evident from the strong relative intensity decrease of the two π^* resonances with respect to the features assigned to states with a strong σ^* character on going from 90° to 0°. The decay dynamics is therefore strongly dependent on the σ/π antibonding character of the resonant state.

Conclusions

The joint experimental and theoretical work presented here provides for the first time a reliable assignment for the core excitation processes in the ozone molecule in the whole spectral range. The high photon resolution, the high purity of the ozone source, and the linear polarization of the light made possible the following: (a) a state selective study of the second experimental band in the TIY spectrum; (b) to observe clearly four experimental bands in the high energy region without a significant O_2 contamination; (c) an experimental characterization of the two states contributing to the second band, the O_C $1s \rightarrow \pi^*(2b_1)$ and O_T $1s \rightarrow \sigma^*(11a')$ resonances, in terms of angular anisotropy of the photofragment emission and different O_2^+/O^+ ion yield ratio.

A reliable theoretical description of the experimental data in terms of excitation energy pattern and photoabsorption oscillator strengths was achieved only using a high level ab initio approach. The assignment of the high energy part of the TIY spectrum was based crucially on the theoretical predictions. Good agreement was found between the experimental and theoretical results. Finally, it was clearly shown that standard theoretical approaches (e.g., 1h−1p CI scheme) giving a satisfactory description of XAS spectra of closed shell molecules do not describe correctly the highly correlated ozone molecule.

Acknowledgment. We gratefully acknowledge Dr. M. Coreno and Dr. M. de Simone for helpful discussions and assistance during the measurements. We are in debt to Dr. R. Richter for his experimental support, stimulating discussions, and a critical revision of the manuscript. We thank the staff of Elettra for technical assistance. The authors gratefully acknowledge financial support by MURST, INFM, and CNR.

References and Notes

(1) Gejo, T.; Okada, K.; Ibuki, T. *Chem. Phys. Lett.* **1997**, *277*, 497−501.
(2) Gejo, T.; Okada, K.; Ibuki, T.; Saito, N. *J. Phys. Chem. A* **1999**, *103*, 4598−4601.
(3) Naves de Brito, A.; Sundin, S.; Marinho, R. R.; Hjelte, I.; Fraguas, G.; Gejo, T.; Kosugi, N.; Sorensen, S.; Bjrneholm, O. *Chem. Phys. Lett.* **2000**, *328*, 177−187.
(4) Wiesner, K.; Rosenqvist, L.; Naves de Brito, A.; M. Bässler, A. Ausmees, R. Feifel, I. Hjelte, S. L. Sorensen, C. Miron, H. Wang, M. N. Piancastelli, S. Svensson, and, O. Björneholm, *Books of Abstracts*, 18th International Conference on X-ray and Inner-Shell Processes, Chicago, August 23−27, 1999; Argonne National Laboratory: Argonne, IL; p 288.
(5) Banna, M. S.; Frost, D. C.; McDowell, C. A.; Noodleman, L.; Wallbank, B. *Chem. Phys. Lett.* **1977**, *49*, 213-217.
(6) Blyth, R. R.; Delaunay, R.; Zitnik, M.; Krempasky, J.; Krempaska, R.; Slezak, J.; Prince, K. C.; Richter, R.; Vondracek, M.; Camilloni, R.; Avaldi, L.; Coreno, M.; Stefani, G.; Furlani, C.; de Simone, M.; Stranges, S.; Adam, M. Y. *J. Electron Spectrosc. Relat. Phenom.* **1999**, *101*−*103*, 959−964.
(7) Yagishita, A.; Shigemasa, E. *Phys. Rev. Lett.* **1994**, *72*, 3961−3964.
(8) Kosugi, N. *J. Electron Spectrosc. Relat. Phenom.* **1996**, *79*, 351−356.
(9) Saito, N.; Suzuki, I. H. *Phys. Rev. A* **1991**, *A43*, 3662−3667.
(10) Bozek, J. D.; Saito, N.; Suzuki, I. H. *Phys. Rev. A* **1995**, *51*, 4563−4574.
(11) Decleva, P.; Fronzoni, G.; Lisini, A.; Stener, M. *Chem. Phys.* **1994**, *186*, 1−16.
(12) Fronzoni, G.; Decleva, P. *Chem. Phys.* **1998**, *237*, 21−42.
(13) Durand, P.; Malrieu, J. P. *Adv. Chem. Phys.* **1987**, *67*, 321−412.
(14) Fronzoni, G.; Stener, M.; Decleva, P. *Chem. Phys.* **1999**, *246*, 127−145, and references therein.
(15) Ma, Y.; Chen, C. T.; Meigs, G.; Randall, K.; Sette, F. *Phys. Rev. A* **1991**, *A44*, 1848−1858.
(16) Hitchcock, A. P.; Brion, C. E. *J. Electron Spectrosc. Relat. Phenom.* **1980**, *18*, 1−21.
(17) Dyke, J. M.; Golob, L.; Jonathan, N.; Morris, A.; Okuda, M. *J. Chem. Soc., Faraday Trans. 2* **1974**, *70*, 1828−1836.
(18) Dunning, T. H. *J. Chem. Phys.* **1989**, *90*, 1007−1022.
(19) Lisini, A.; Decleva, P.; Fronzoni, G. *Chem. Phys.* **1993**, *171*, 159−170.
(20) Fronzoni, G.; Decleva, P. *Chem. Phys.* **1997**, *220*, 15−24 and references therein.
(21) Davidson, E. R.; MELDF, QCPE Program 580. *QCPE Bull.* **1989**, *9*, 98.
(22) Syage, J. A. *J. Chem. Phys.* **1996**, *105*, 1007−1022.
(23) Bergmann, K.; Carter, R. T.; Hall, G. E.; Huber, J. R. *J. Chem. Phys.* **1998**, *109*, 474−483.
(24) Larsson, M.; Baltzer, P.; Svensson, S.; Wannberg, B.; Mårtensson, N.; Naves de Brito, A.; Correia, N.; Keane, M. P.; Carlsson-Göthe, M.; Karlsson, L. *J. Phys. B.* **1990**, *23*, 1175−1195.